(2)

LOW-SPEED CHARACTERISTICS OF A CIRCULATION CONTROL AIRFOIL WITH AFT CAMBER AND A SPIRAL TRAILING EDGE

by

Jane Abramson

AVIATION AND SURFACE EFFECTS DEPARTMENT

DTNSRDC/ASED-84/07

December 1984

DAVID W. TAYLOR NAVAL SHIP RESEARCH AND DEVELOPMENT CENTER

BETHESDA
MARYLAND
20084

UNCLASSIFIED

SECURITY CLASSIFICATION OF THIS PAGE (When Data Entered)

REPORT DOCUMENTATION PAGE		READ INSTRUCTIONS BEFORE COMPLETING FORM
1. REPORT NUMBER DTNSRDC/ASED-84/07	2. GOVT ACCESSION NO.	3. RECIPIENT'S CATALOG NUMBER
4. TITLE (and Subtitle) LOW-SPEED CHARACTERISTICS OF A CIRCULATION CONTROL AIRFOIL WITH AFT CAMBER AND A SPIRAL TRAILING EDGE		5. TYPE OF REPORT & PERIOD COVERED Final 6. PERFORMING ORG. REPORT NUMBER
7. AUTHOR(s) Jane Abramson		8. CONTRACT OR GRANT NUMBER(s)
9. PERFORMING ORGANIZATION NAME AND ADDRESS David W. Taylor Naval Ship R&D Center Aviation and Surface Effects Department Bethesda, Maryland 20084		10. PROGRAM ELEMENT, PROJECT, TASK AREA & WORK UNIT NUMBERS Project Element 63203N Task Area W0578 Work Unit 1619-300
11. CONTROLLING OFFICE NAME AND ADDRESS Naval Air Systems Command AIR-310 Washington, D.C. 20361		12. REPORT DATE December 1984 13. NUMBER OF PAGES 40
14. MONITORING AGENCY NAME & ADDRESS(if different from Controlling Office)		15. SECURITY CLASS. (of this report) UNCLASSIFIED 15a. DECLASSIFICATION/DOWNGRADING SCHEDULE

16. DISTRIBUTION STATEMENT (of this Report)

APPROVED FOR PUBLIC RELEASE: DISTRIBUTION UNLIMITED

17. DISTRIBUTION STATEMENT (of the abstract entered in Block 20, if different from Report)

18. SUPPLEMENTARY NOTES

19. KEY WORDS (Continue on reverse side if necessary and identify by block number)

Two-Dimensional Wind Tunnel Testing
Circulation Control Airfoil
Tangential Blowing
Boundary Layer Control

20. ABSTRACT (Continue on reverse side if necessary and identify by block number)

A circulation control elliptic airfoil section with a 15-percent thickness-to-chord ratio which incorporates a spiral trailing edge was evaluated subsonically to determine its aerodynamic characteristics. The spiral-shaped Coanda surface was previously evaluated with a different leading edge. The airfoil, designated NCCR 1505-7567S, has an uncambered forward half and a cambered aft portion resulting in a 0.605-percent camber

DD FORM 1 JAN 73 1473 EDITION OF 1 NOV 65 IS OBSOLETE
S/N 0102-LF-014-6601

UNCLASSIFIED

SECURITY CLASSIFICATION OF THIS PAGE (When Data Entered)

for the profile. This particular combination of camber was selected because it was analytically predicted to have good critical Mach number characteristics in the range of interest. The range of momentum coefficient was limited due to the relatively early onset of Coanda jet-tunnel floor interference; however, lift coefficients in excess of 4.25 were produced at momentum coefficients of 0.16. Equivalent lift-to-drag ratios in excess of 40 were also produced when lift coefficient reached approximately 1.0. Originator-supplied Keywords → (te... 23 A.)

TABLE OF CONTENTS

	Page
LIST OF FIGURES	iii
LIST OF TABLES	iv
NOTATION	v
ABSTRACT	1
ADMINISTRATIVE INFORMATION	1
INTRODUCTION	1
MODEL AND TEST APPARATUS	2
RESULTS AND DISCUSSION	5
LIFT	6
DRAG	8
PITCHING MOMENT	8
EQUIVALENT LIFT-TO-DRAG RATIO	8
CONCLUSIONS	10
REFERENCES	11

LIST OF FIGURES

1 - Two-Dimensional Model	13
2 - Lift Variation with Dynamic Pressure	14
3 - Variation of Momentum Coefficient with Duct Pressure and Slot Height	15
4 - Variation of Slot Height with Duct Pressure	16
5 - Lift Variation with Momentum Coefficient	17
6 - Lift Variation with the Square Root of Momentum Coefficient	21
7 - Experimental Pressure Distributions at α = -20 Degrees	22
8 - Variation of Lift Augmentation with Momentum Coefficient	23
9 - Lift Variation with Geometric Angle of Attack	25
10 - Minimum Pressure Coefficient at h/c = 0.0015	26

Page

11 - Variation of Estimated Critical Mach Number with Lift Coefficient 27

12 - Induced Angle Correction to Geometric Incidence 28

13 - Drag Coefficient Variation with Momentum Coefficient 29

14 - Variation in Half-Chord Pitching Moment Coefficient at h/c = 0.0015 32

15 - Equivalent Lift-to-Drag Ratio 33

LIST OF TABLES

1 - Designation of CCR Airfoils 3

2 - Two-Dimensional Model Coordinates for Upper and Lower Surfaces 4

NOTATION

a_j	Sonic velocity in the jet
C_d	Sectional profile drag coefficient from momentum loss in wake, corrected for additional mass efflux of the jet
$C_{d_{rake}}$	Section profile drag coefficient as measured by rake, uncorrected for jet efflux effects
C_ℓ	Sectional lift coefficient
$C_{\ell_{max}}$	Maximum sectional lift coefficient obtainable within test C_μ limitations
$C_{m_{50}}$	Pitching moment coefficient about the midchord
C_P	Pressure coefficient
C_μ	Momentum coefficient
c	Chord length
d	Sectional profile drag corrected for jet mass efflux
d_e	Sectional equivalent drag
h/c	Slot height-to-chord ratio
ℓ/d_e	Equivalent section lift-to-drag ratio
M_{crit}	Critical Mach number
M_j	Jet Mach number
$\dot{m}$	Mass efflux, slugs/sec
P_d	Duct (plenum) total pressure
P_{t_∞}	Free-stream total pressure
P_∞	Free-stream static pressure
q_∞	Free-stream dynamic pressure
R	Universal gas constant
s	Model planform area
T_d	Duct (plenum) total temperature, °R

V_j	Jet velocity
V_∞	Free-stream velocity
x/c	Dimensionless chordwise position
α	Geometric angle of attack
γ	Ratio of specific heats

ABSTRACT

A circulation control elliptic airfoil section with a 15-percent thickness-to-chord ratio which incorporates a spiral trailing edge was evaluated subsonically to determine its aerodynamic characteristics. The spiral-shaped Coanda surface was previously evaluated with a different leading edge. The airfoil designated NCCR 1505-7567S has an uncambered forward half and a cambered aft portion resulting in a 0.005-percent camber for the profile. This particular combination of camber was selected because it was analytically predicted to have good critical Mach number characteristics in the range of interest. The range of momentum coefficient was limited due to the relatively early onset of Coanda jet-tunnel floor interference; however, lift coefficients in excess of 4.25 were produced at momentum coefficients of 0.16. Equivalent lift-to-drag ratios in excess of 40 were also produced when lift coefficient reached approximately 1.0.

ADMINISTRATIVE INFORMATION

The work presented was conducted in 1976 at the David W. Taylor Naval Ship Research and Development Center (DTNSRDC) for the Naval Air Systems Command (AIR-320D) under Project Element 63203N and Task Area W0578.

INTRODUCTION

Tangential blowing over the bluff trailing edge of elliptical airfoil sections has been shown to produce high-lift augmentation at relatively low blowing levels over a range of angles of attack. Because of the Coanda effect employed by these airfoils, the jet sheet remains attached to the bluff trailing edge due to a balance between the centrifugal force and the reduced pressure at the wall. Initially, the Coanda jet acts as an effective boundary layer control mechanism by entraining the upstream flow. At the higher blowing rates, there is substantial movement of the stagnation points with an accompanying increase in circulation.

In the present investigation, the subsonic characteristics of a 15-percent cambered elliptic airfoil section are experimentally examined. The airfoil is one of a series of five being used in a circulation control airfoil development program at DTNSRDC to determine the effect of leading and trailing edge geometry on performance.[1-3]* The Coanda surface employed on this airfoil is the same as that evaluated previously on model NCCR 1510-7567S.[2]

*A complete listing of references is given on page 11.

MODEL AND TEST APPARATUS

The airfoil profile designated NCCR 1505-7567S is based on an analytically defined ellipse with an 8-in. major axis (chord) and a 15-percent thickness-to-chord ratio; see Table 1. Modifying the ellipse to produce the desired Coanda surface trailing edge shape reduces the chord to 7.991 in. An upper surface jet slot is placed at the 0.97-percent chord position. The forward portion of the model, $x/c \leq 0.5$, is uncambered with a leading edge radius-to-chord ratio of 0.02137, which is 190 percent that of the pure ellipse. For $x/c \geq 0.5$, a circular arc camber of 0.01 percent was applied. This particular combination of camber was selected because the airfoil was analytically predicted to reach critical Mach number outside a selected range of lift coefficients and angles of incidence. Also, the cambered aft portion was available from a model previously evaluated. Coordinates as input for model construction are listed in Table 2.

The outer shell of the model is constructed of wood with an internal steel plenum chamber through which air for the Coanda jet is introduced. The jet (slot) exit is the throat of a converging nozzle formed by the internal geometry of the Coanda surface and the underside of a knife-edged aluminum blade. The Coanda surface itself is a spiral with the smallest radius of curvature at the slot. An undercut surface is used on the aluminum blade to ensure that the flow will exit tantentially to the airfoil surface; see Figure 1. Slot height is adjusted through the use of pitch screws.

Two-dimensional tests were conducted in the 15- by 20-in. subsonic wind tunnel with a vented test section and plexiglass walls. The model was pressure-tapped at center span. Lift and pitching moment coefficients were obtained by numerical integration of pressure tap readings as recorded on a multiple-port scanivalve readout system. These coefficients were corrected by the addition of jet reaction components. Standard solid blockage corrections[4] were applied to the measured free-stream dynamic pressure; no wake blockage factor was used because of the uncertain effects of the jet.

Drag measurements were made by using a drag rake placed approximately 1.5 chord lengths downstream of the model inclined at 10 deg to the free stream. The rake employs 54 total and 8 static tubes, with the heaviest concentration of tubes near the center height. The momentum deficit methods of Betz and Jones[5] were then used to determine the drag coefficient. Since neither method accounts for the additional momentum introduced by the jet, a term of $\dot{m}V_j/q_\infty s$ was subtracted from the calculated drag.

TABLE 1 — DESIGNATION FOR CCR AIRFOILS

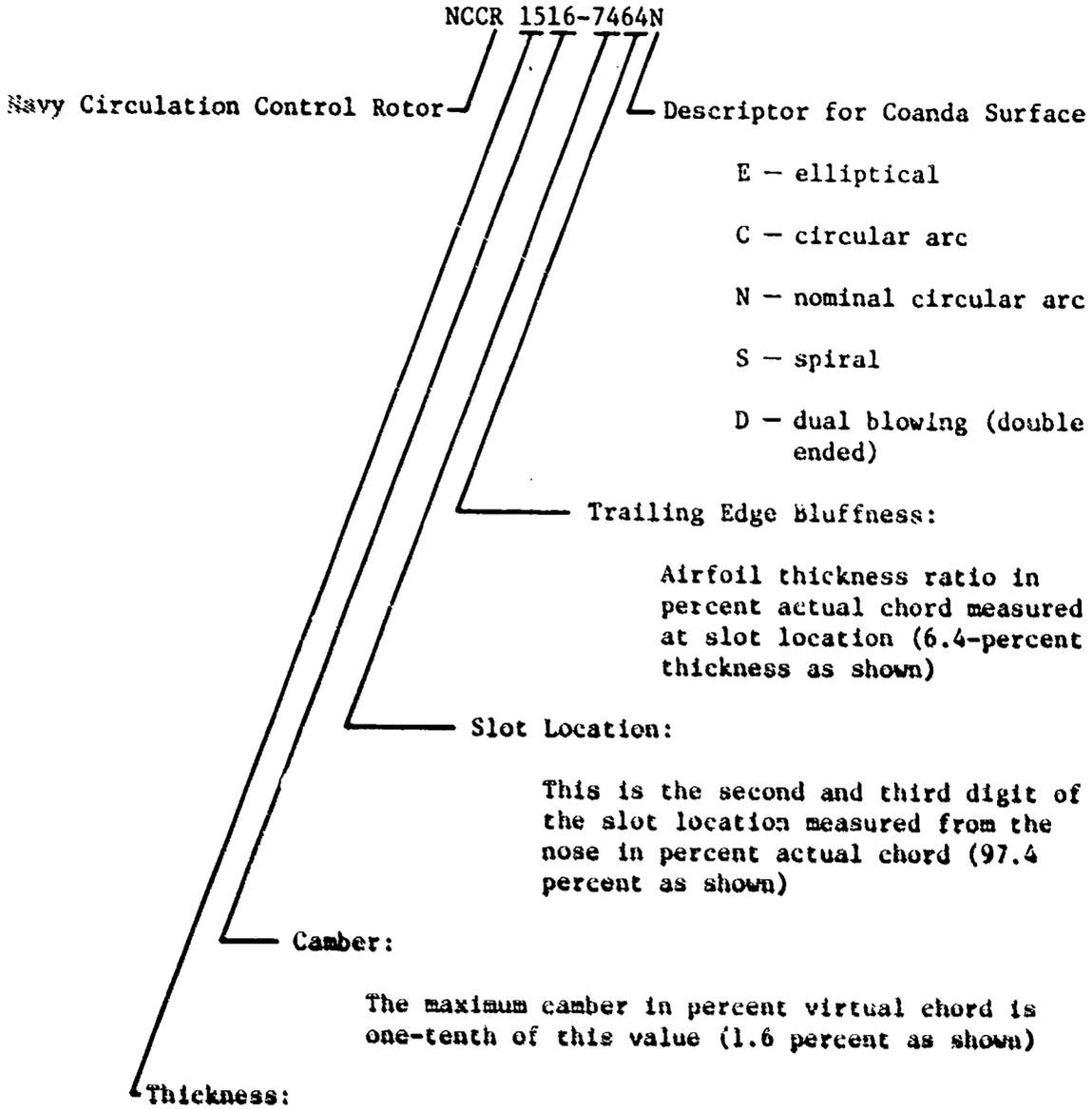

TABLE 2 - Two-Dimensional Model Coordinates for Upper and Lower Surfaces

UPPER SURFACE			LOWER SURFACE	
X	Y		X	Y
0	0.081	LEADING EDGE	0	0.081
0.010	0.141		0.010	0.020
0.030	0.181		0.020	0.000
0.050	0.205		0.040	−0.031
0.072	0.225		0.060	−0.051
0.129	0.257		0.129	−0.093
0.243	0.306		0.243	−0.143
0.357	0.346		0.[illegible]	−0.182
0.584	0.408		0.527	−0.230
0.811	0.456		0.754	−0.282
1.038	0.497		1.095	−0.342
1.379	0.546		1.436	−0.396
1.890	0.603		2.118	−0.459
2.345	0.639		2.743	−0.499
2.800	0.666		3.368	−0.523
3.254	0.684		3.822	−0.531
3.709	0.693		4.429	−0.529
4.050	0.695		5.152	−0.515
4.795	0.682		5.876	−0.484
5.209	0.664		6.601	−0.428
5.860	0.616		7.100	−0.369
6.230	0.579		7.329	−0.335
6.950	0.474		7.457	−0.312
7.360	0.392		7.603	−0.281
7.502	0.355		7.750	−0.225
7.647	0.314		7.810	−0.180
7.719	0.290		7.850	−0.138
7.750	0.265		7.890	−0.070
7.810	0.239		7.910	−0.010
7.890	0.151		7.915	0.040
7.915	0.040	TRAILING EDGE		

To ensure that test conditions were as close to two-dimensional flow as possible (especially at high-lift conditions), wall blowing was employed. Two sets of plenums were embedded in each of the tunnel walls—one ahead of the leading edge, the other at approximately the 70-percent chord position. The blowing rates of the two sets of wall jets were adjusted independently and in accordance with the model blowing rate. The wall jets were used to energize the wall boundary layer to prevent separation and reduce the vorticity associated with induced effects. Spanwise pressure taps were employed to record the lateral pressure distribution as an indication of two-dimensionality.

The level of blowing is expressed by the momentum coefficient, C_μ, where

$$C_\mu = \dot{m}V_j/(q_\infty s)$$

Mass flow rate, $\dot{m}$, was measured by a calibrated orifice plate inserted in the supply line. Jet velocity was calculated by assuming isentropic expansion from duct stagnation pressure to the free-stream static pressure as follows:

$$V_j = a_j M_j = \left\{2RT_d \left(\frac{\gamma}{\gamma-1}\right) \left[1-\left(\frac{P_\infty}{P_d}\right)^{\gamma-1/\gamma}\right]\right\}^{1/2}$$

A series of runs were made at free-stream dynamic pressures from 20 to 50 lb/ft^2 corresponding to a model Reynolds number range from 0.524×10^6 to 0.825×10^6 (Figure 2). No significant effect on the data over this Reynolds number range was noted, and $q_\infty = 20$ lb/ft^2 was chosen to allow for a wider range of C_μ, due to limits on the allowable internal duct pressure.

RESULTS AND DISCUSSION

The characteristics of a modified cambered 15-percent ellipse with a spiral trailing edge was evaluated for three slot height-to-chord ratios of 0.0015, 0.0010, and 0.0022 for angles of attack of -20 to 10 deg and momentum coefficients ranging from 0 to 0.165. The range of the momentum coefficient is somewhat limited due to the relatively early onset of jet-tunnel floor interference. Figure 3 depicts the variation of momentum coefficient with duct pressure for the three slot height-to-chord ratios for the test dynamic pressure of 20 lb/ft^2. The expansion of the slot caused by pressurization of the duct at h/c = 0.0015 is shown in Figure 4. These

data were obtained by pressurizing the duct and measuring the resulting slot height with a thickness gage under quiescent tunnel conditions.

LIFT

Figures 5a and 5b show the sectional lift coefficient as a function of momentum coefficient for h/c = 0.0015, 0.0010, and 0.0022. The data are also presented on an expanded scale and as a function of the square root of the momentum coefficient in Figures 5c, 5d, and 6. Although all recorded data are included for completeness, a hatch mark appears in these figures to indicate the point at which disturbance of a set of floor tufts placed behind the model was visually noted, indicating the onset of jet-tunnel floor interference. There is, of course, the possibility that interference effects are occurring at lower C_μ values. The general level of disturbance in the tunnel was high at α = +10 and -20 deg; therefore, no definitive interference point could be observed.

For h/c = 0.0015, as indicated in Figure 5a, maximum lift coefficient occurs at progressively lower values of momentum coefficient at α = 0, 2, 6, and 10 deg; this coincides with a loss in the leading edge suction peak. For the negative angles of incidence, the lift coefficient continues to increase with increasing C_μ. Maximum lift coefficient for this airfoil is 4.28 reached at α = -2 deg for C_μ = 0.159. A brief experiment was performed, and results indicated that higher values of $C_{\ell_{max}}$ can be generated, if sufficient clearance between the model and the tunnel floor can be provided. At α = -2, -4, and -8 deg, the pressure distributions do not reveal any evidence of lower leading edge separation bubbles; however, at α = -12 deg under nonblowing conditions, such a separation bubble does exist. Initially, the flow is separated along the entire lower surface of α = -20 deg. As blowing increases, the stagnation point (which is on the upper surface) moves forward toward the leading edge, resulting in flow attachment at $C_\mu \approx 0.09$; see Figure 7. Despite the presence of separated flow, positive values of lift coefficient are produced for $C_\mu \geq 0.04$.

A comparison of lift characteristics in Figures 5a and 5b for the three slot heights shows that, in general, a higher lift coefficient is obtained for a given momentum coefficient at h/c = 0.0015. An exception to this is observed when comparing the low momentum coefficient data on the expanded scale plots of Figures 5c and 5d. In this range, the h/c = 0.0010 data show either the same or improved

performance in relation to the larger slot height at the incidences tested. The relative performance of the model at h/c = 0.0010 and 0.0022 (Figure 5b), however, must be viewed with caution. The lift produced at the two slot heights is approximately the same until the region at which floor impingement is noted at h/c = 0.0010.

Figures 8a and 8b depict the augmentation ratio as a function of momentum coefficient. Augmentation ratio is defined at $\Delta C_\ell / C_\mu$, where ΔC_ℓ is the increase in lift coefficient above the unblown value for a given C_μ and incidence. A significant reduction in augmentation ratio is apparent in Figure 8a at α = -20 and +10 deg and to a lesser extent at α = 6 deg; the remaining data fall within a narrow band. In comparing the results in Figures 8a and 8b, the highest maximum augmentation is found to occur at h/c = 0.0010. This is the result of the increased lift coefficient achieved at low values of momentum coefficient at this slot height.

Variation of lift coefficient with geometric angle of attack is shown in Figure 9. The slope of the curves is similar for nonstall conditions, indicating that the relationship between lift coefficient and incidence is not influenced by the level of blowing. Good agreement is seen between the unblown case and the theoretical value of lift predicted for conventional airfoils.

The minimum value of pressure coefficient, $C_{p_{min}}$, on the airfoil as a function of lift coefficient is depicted in Figure 10. Critical Mach number for the airfoil is predicted by applying the Kaman-Tsien compressibility correction to these values of $C_{p_{min}}$. Figure 11 presents M_{crit} as a function of the compressible lift coefficient, $CC_\ell = C_\ell / (1-M_{crit}^2)^{1/2}$. Compressibility factor techniques such as Kaman-Tsien do not fully account for the effect of compressibility, particularly in a region of high acceleration; see Reference 5. Nonetheless, this prediction is useful as an indication of high-speed performance. Figure 11 indicates a maximum M_{crit} in excess of 0.70 at both α = 0 and -2 deg for a range of lift coefficients.

To complete the discussion of lift characteristics, the effect of spanwise nonuniformity must be considered. Although wall blowing was used to ensure spanwise two-dimensionality, the high-lift coefficients still produced downwash. Thus, a determination of the effective angle of incidence was made. For the experimental cases selected, potential flow pressure distributions for several incidences and the experimental C_ℓ were determined. The resulting distributions were then compared to the experimental pressure distribution until leading edge characteristics coincided.

The effective angles of incidence for the experimental data are presented in Figure 12.

DRAG

The variation of a modified drag coefficient with momentum coefficient is presented in Figures 13a and 13b for h/c = 0.0015, 0.0010 and 0.0022. Data at low values of momentum coefficient on an expanded scale for h/c = 0.0015 are shown in Figure 13c. These data result from an integration of the wake deficit using the method of Betz[4] which was modified to account for the additional momentum of the jet, $C_d = C_{d_{wake}} - (\dot{m}V_\infty/qs)$. The initial unblown drag levels are high due to the nature of bluff trailing edge airfoils; however, with the onset of blowing a reduction in drag is noted at most angles of attack. Negative drag levels, a product of effective thrust recovery, are achieved at relatively low values of momentum for all negative angles of incidence except at $\alpha = -20$ deg. Extensive flow separation on the airfoil lower surface at $\alpha = -20$ deg results in this high drag level.

A reduction in the unblown drag level does not occur at $\alpha = 10$ deg. In this case, the leading edge bubble, which was followed by stall, tended to prevent drag reduction. The secondary drag rise at $\alpha = 10$, 6, and 2 deg coincides with the degradation in lift coefficient observed in Figure 5a. Drag rise is also noted for all points where jet-tunnel floor interference is known to occur.

PITCHING MOMENT

Pitching moment is obtained by an integration of surface pressures. Figure 14 presents the moment about the midchord, $C_{m_{50}}$, as a function of momentum coefficient. The lift due-to-blowing vector is generally located somewhat aft of the midchord because of the suction generated over the trailing edge. Augmented lift therefore produces a negative pitching moment.

EQUIVALENT LIFT-TO-DRAG RATIO

An equivalent lift-to-drag ratio, ℓ/d_e, is defined which takes into account the energy expended to produce blowing. Using ℓ/d_e allows a direct comparison to be made between the performance of a circulation control airfoil and an unblown

airfoil. The equivalent drag is defined as:

$$d_e = d + \frac{P_{comp}}{V_\infty} + \dot{m}V_\infty$$

The first term d is the momentum deficit as measured by the drag rake (corrected for jet efflux). The second term accounts for the compressor power (kinetic energy flux), and the third term is an intake momentum flux (ram penalty).

The compressor power required may be expressed as:

$$P_{comp} = \frac{\dot{m}}{2}\left(\frac{2\gamma}{\gamma-1}\right) RT_d \left[1-\left(\frac{P_{ram}}{P_d}\right)^{(\gamma-1)/\gamma}\right]$$

If intake losses are assumed to be negligible, then the ram pressure is equal to the free-stream total pressure. For subsonic flows with $M_\infty \leq 0.2$, $P_{t_\infty} = P_\infty$. Thus, the above equation becomes:

$$P_{comp} = \frac{1}{2}\dot{m}V_j^2$$

Substituting for P_{comp}, the coefficient form is then:

$$\frac{l}{d_e} = C_l \Big/ \left(C_d + C_\mu \frac{V_j}{2V_\infty} + C_\mu \frac{V_\infty}{V_j}\right)$$

Figures 15a and 15b present the lift-to-equivalent drag as a function of lift coefficient for the three slot height-to-chord ratios. The maximum l/d_e generated is approximately 45 at $C_\ell = 0.7$, despite the relatively high-lift coefficients which are generated. Maximum efficiency at a given angle of incidence is produced at low values of momentum coefficient. This emphasizes the need to produce high values of lift coefficient at low values of momentum coefficient to maintain high efficiency due to the prominence of the kinetic energy term, $C_\mu V_j/2V_\infty$.

Comparing the results for the various slot height-to-chord ratios shows that maximum efficiency occurs at h/c = 0.0015, with lower, but similar, results for the remaining slot heights.

CONCLUSIONS

A 15-percent-thick cambered circulation control airfoil was evaluated subsonically. The following conclusions are drawn from the experimental data.

- A maximum lift coefficient of 4.28 is reached at α = -2 deg for C_μ = 0.159. The experimental results indicate that still higher values of maximum lift coefficient can be generated if sufficient clearance between the model and the tunnel floor can be provided.
- The model generated a maximum ℓ/d_e of 45 at C_ℓ = 0.7. Maximum efficiency occurs at positive angles of incidence and low values of momentum coefficient.
- Neither increasing nor decreasing the slot height-to-chord ratio increases the sectional lift coefficient over that obtained at h/c = 0.0015.
- Application of the Karman-Tsien compressibility correction to the experimental values of $C_{p_{min}}$ indicates that the critical Mach number is in excess of 0.7 at both α = 0 and -2 deg.

REFERENCES

1. Wilkerson, J.B., "An Assessment of Circulation Control Airfoil Development," DTNSRDC Report 77-0084 (Aug 1977).

2. Abramson, J., "Two-Dimensional Subsonic Wind Tunnel Evaluation of Two Related Cambered 15-Percent-Thick Circulation Control Airfoils," Report DTNSRDC/ASED-373 (Sep 1977).

3. Abramson, J., "Two Low-Speed Characteristics of a 15-Percent Quasi-Elliptical Circulation Control Airfoil with Distributed Camber," Report DTNSRDC/ASED-79/07 (May 1979).

4. Pope, A., "Wind-Tunnel Testing," Second Edition, John Wiley and Sons, Inc., New York (1964), pp. 307-311.

5. Schichting, Hermann, "Boundary Layer Theory," Sixth Edition, McGraw-Hill Book Company, New York (1968), pp. 708-713.

THIS
PAGE
IS
MISSING
IN
ORIGINAL
DOCUMENT

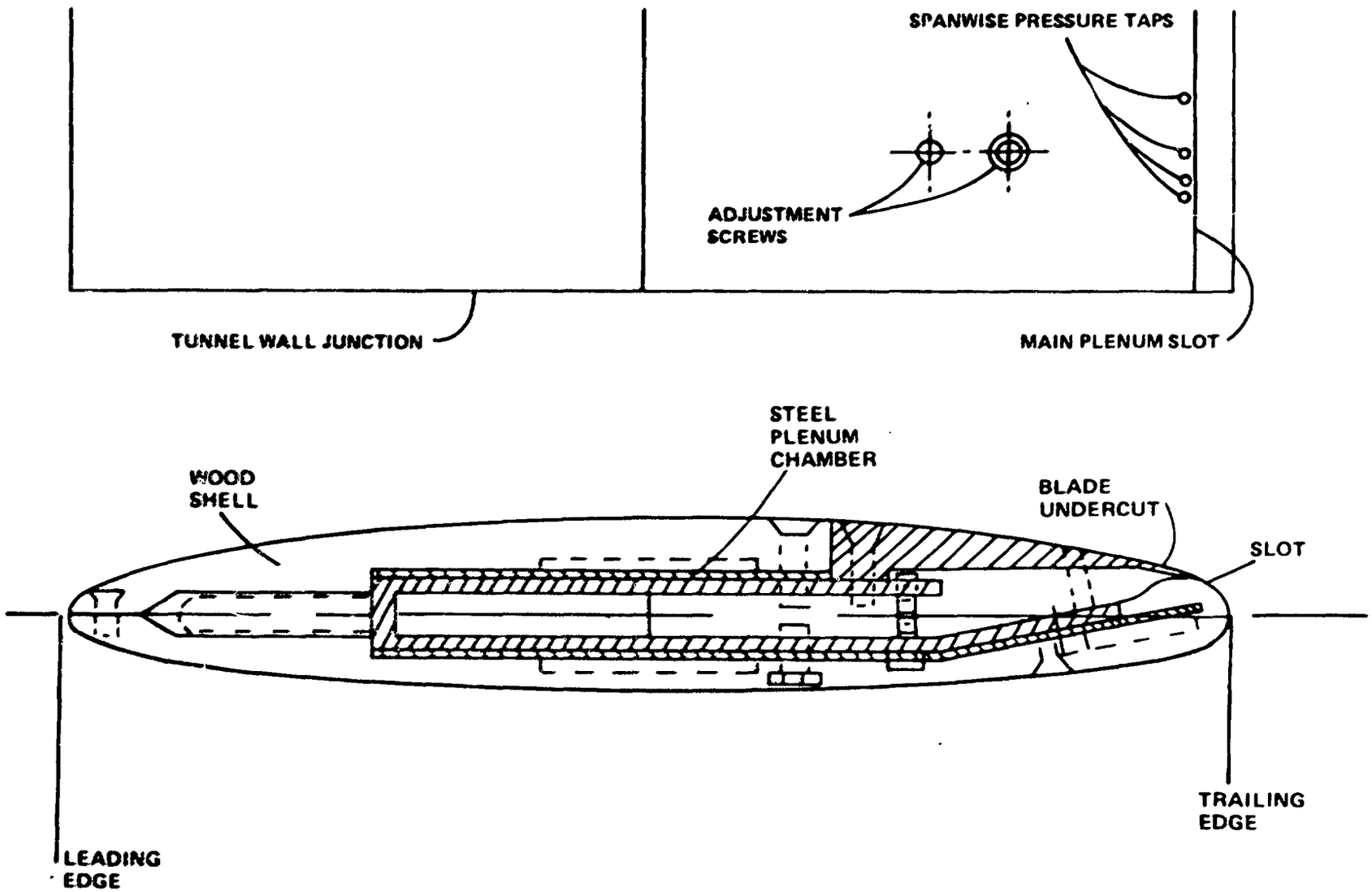

Figure 1 - Two-Dimensional Model Geometry

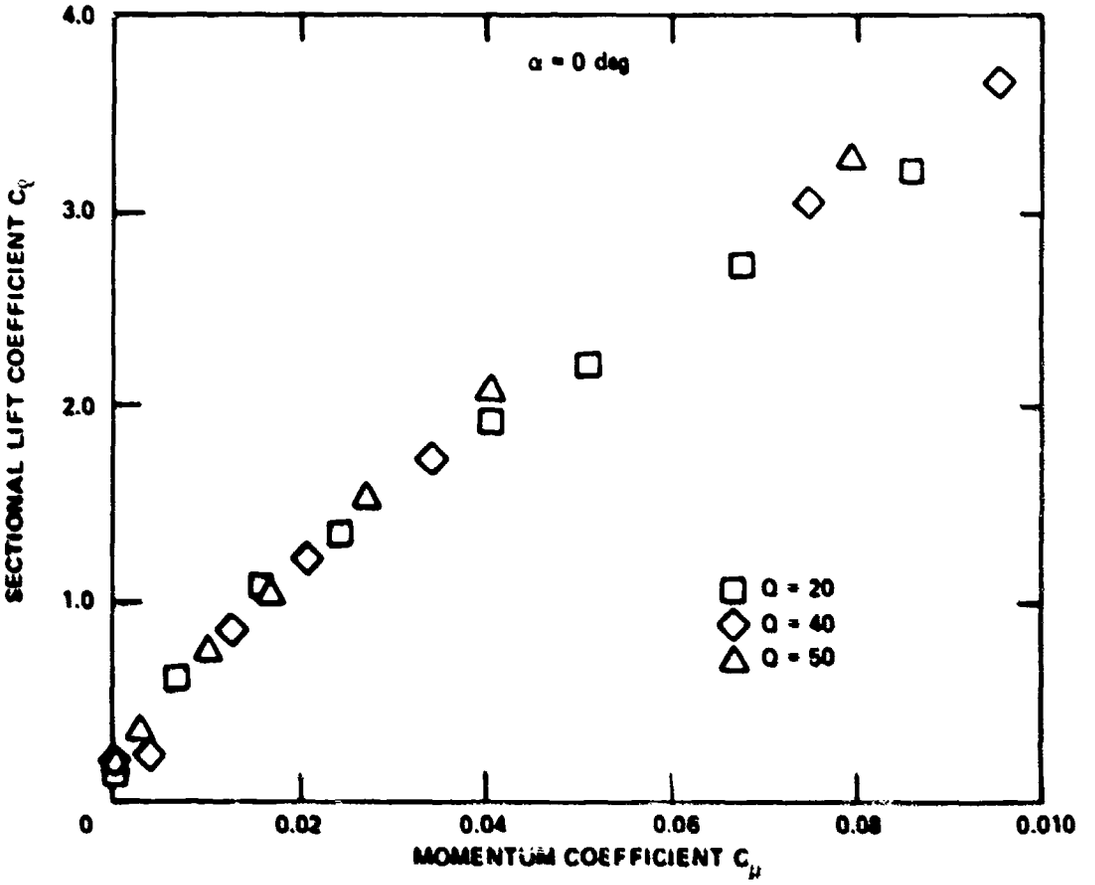

Figure 2 - Lift Variation with Dynamic Pressure

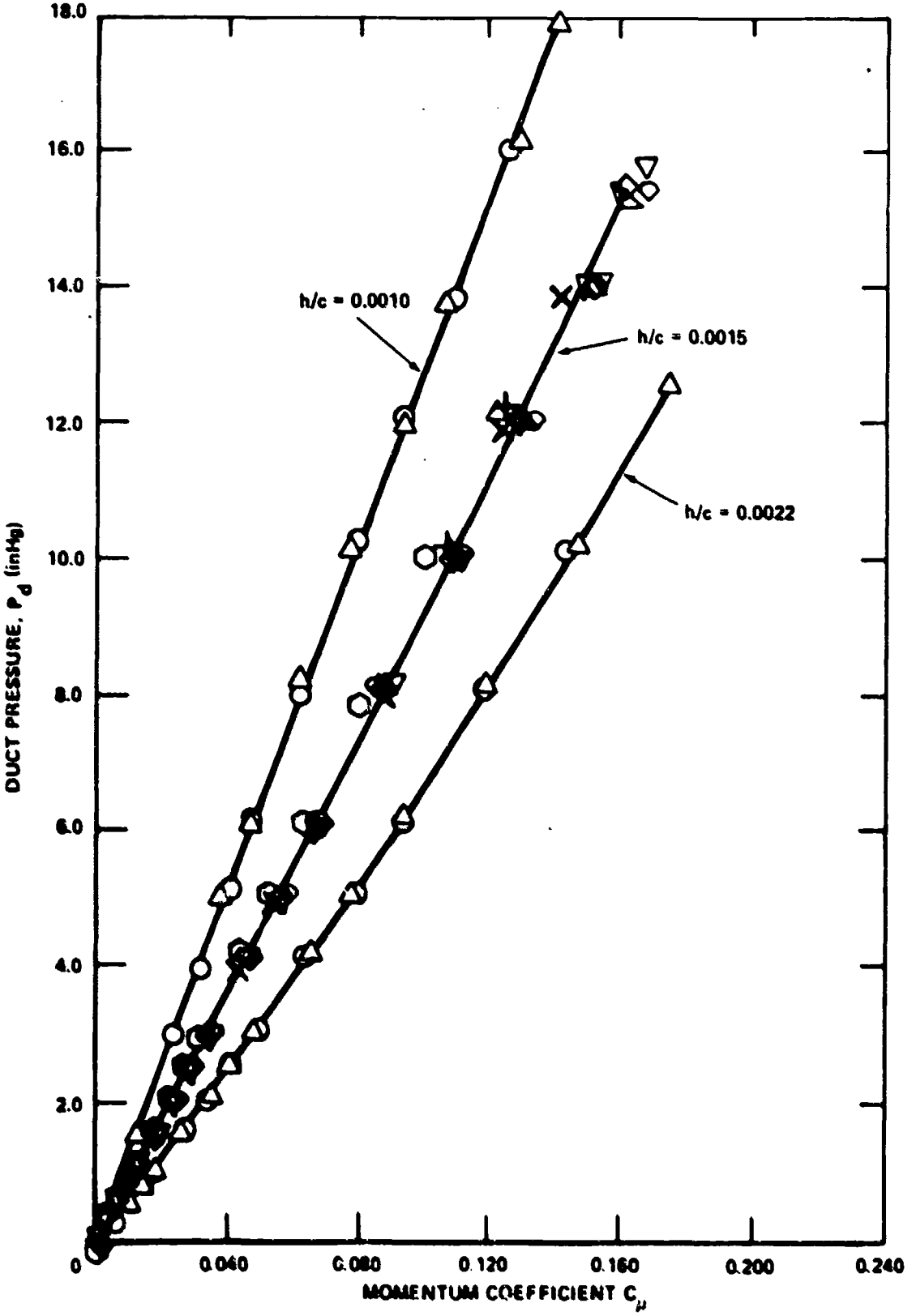

Figure 3 - Variation of Momentum Coefficient with Duct Pressure and Slot Height

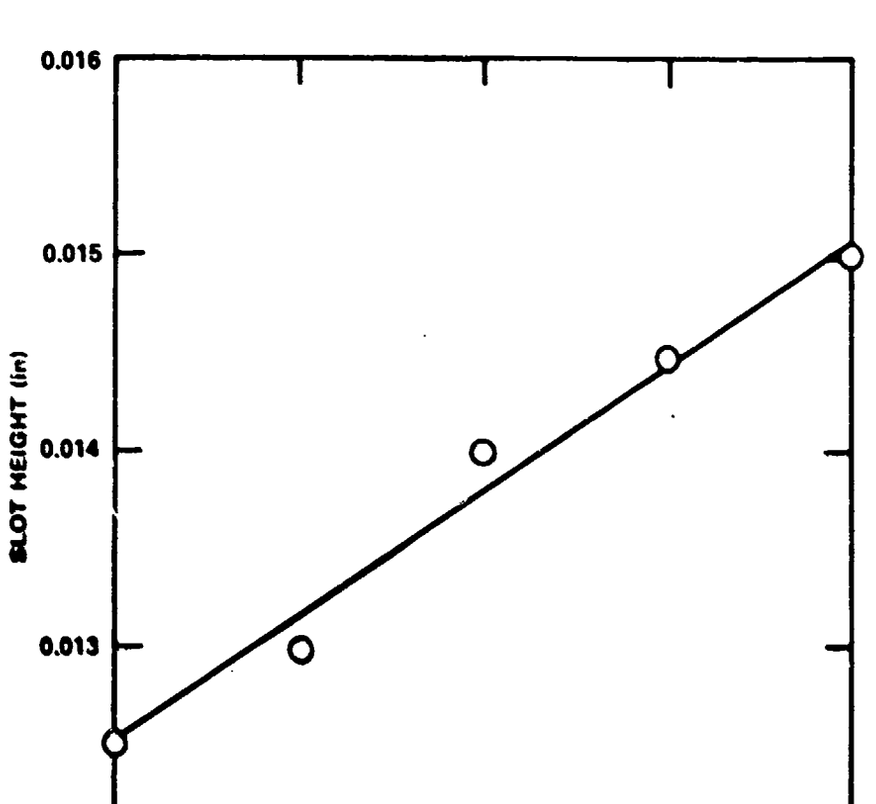

Figure 4 - Variation of Slot Height with Duct Pressure

Figure 5 - Lift Variation with Momentum Coefficient

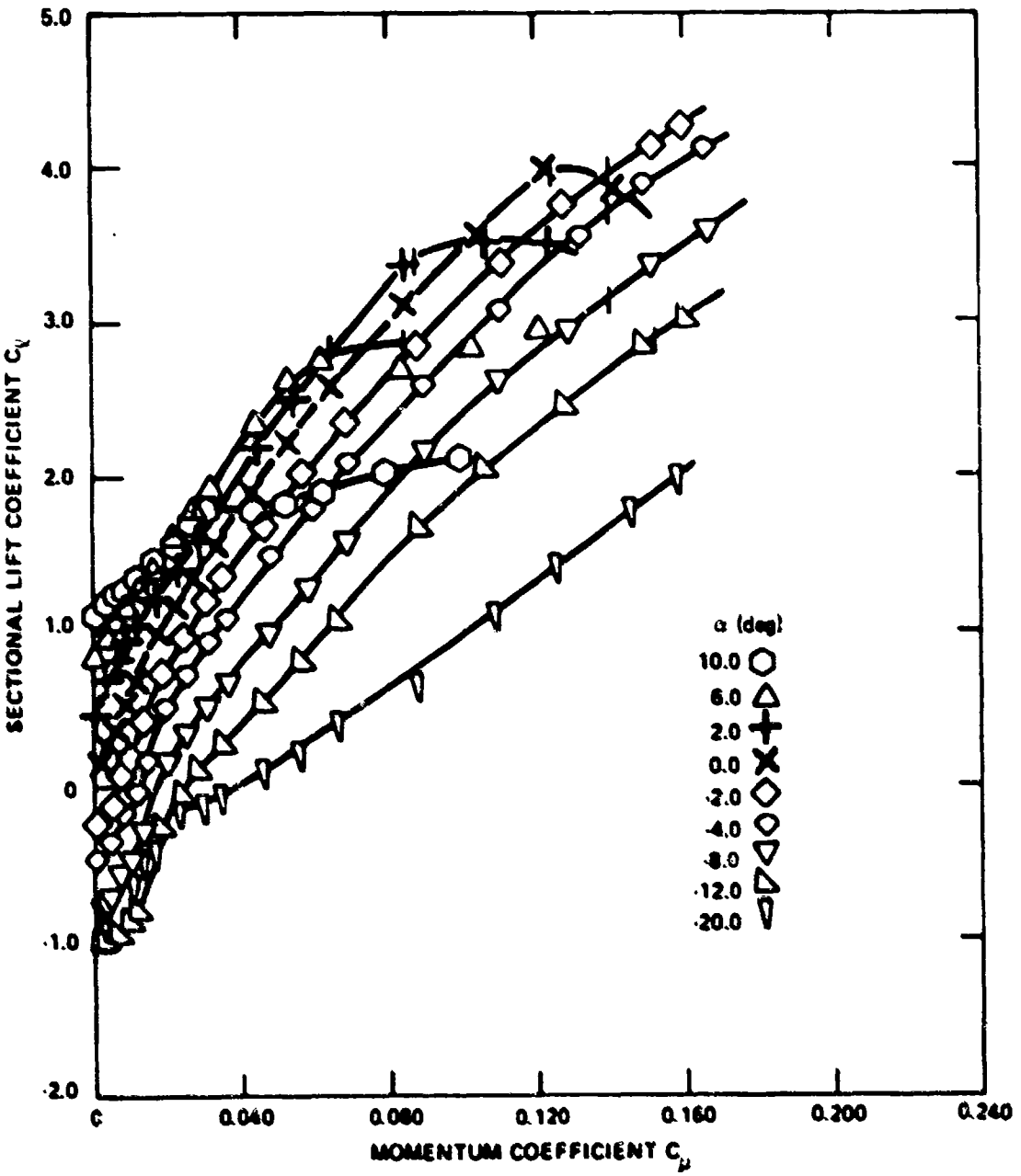

Figure 5a - h/c = 0.0015

Figure 5 (Continued)

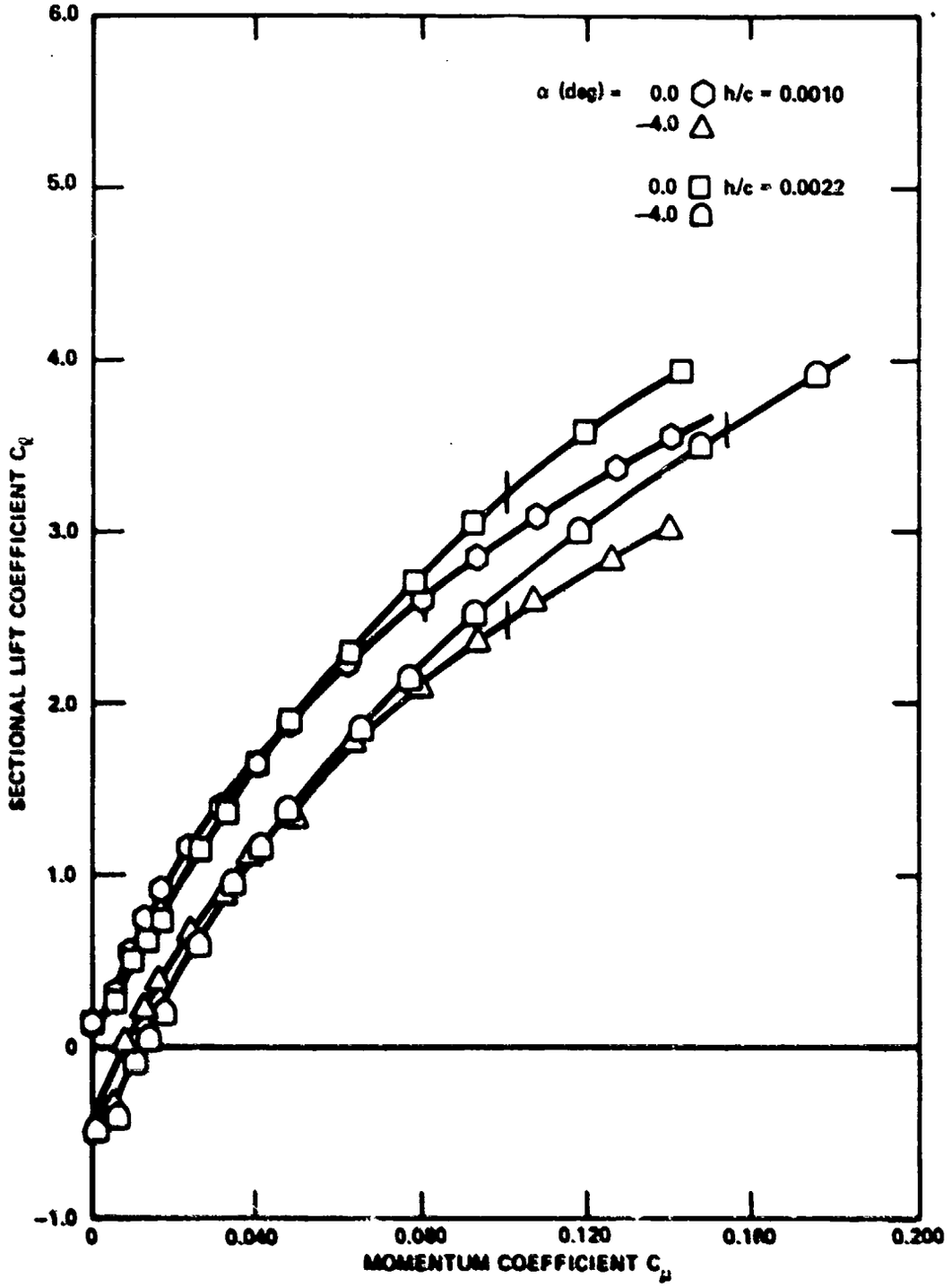

Figure 5b - h/c = 0.0010 and 0.0022

Figure 5 (Continued)

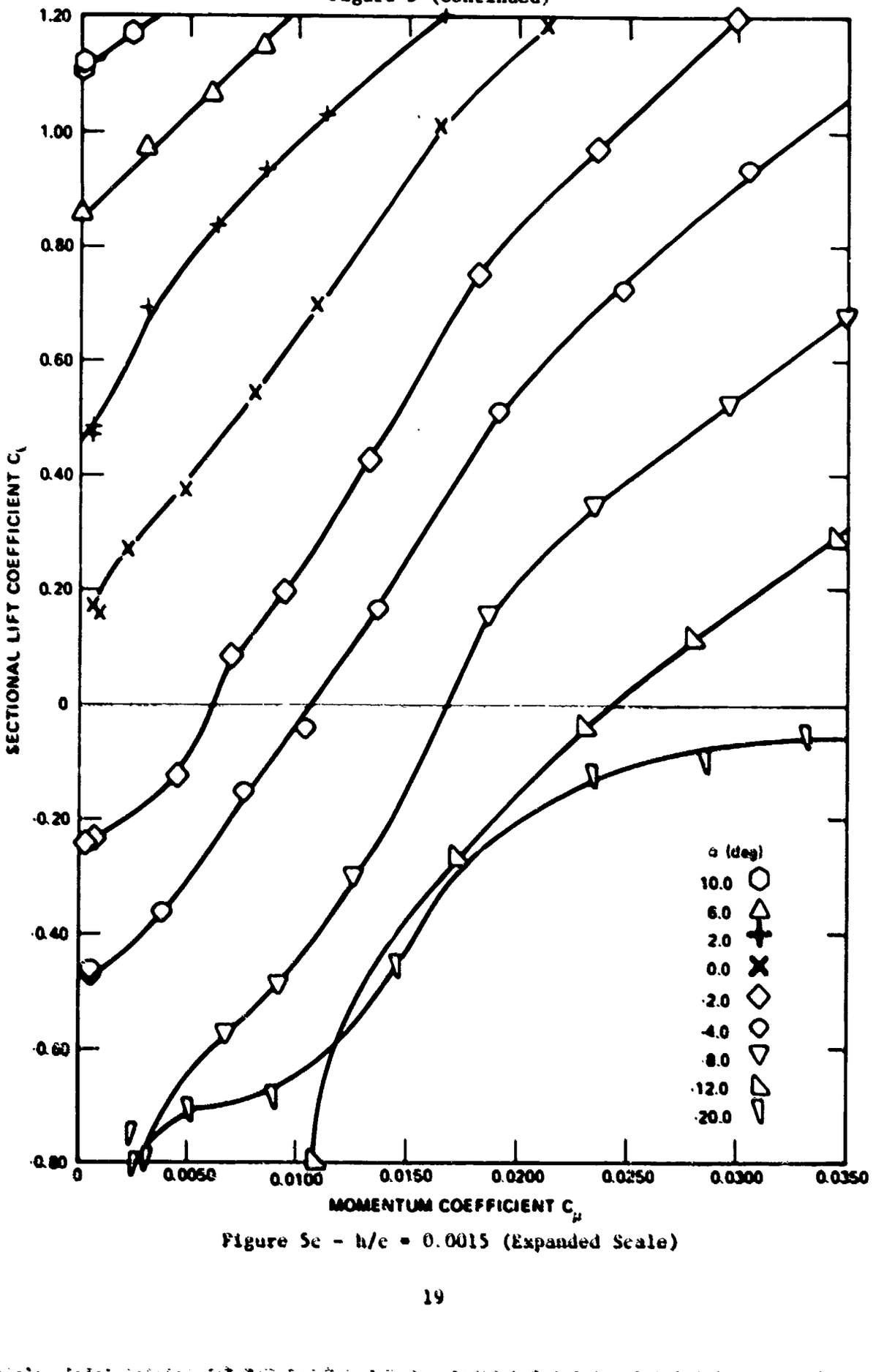

Figure 5c - h/c = 0.0015 (Expanded Scale)

Figure 5 (Continued)

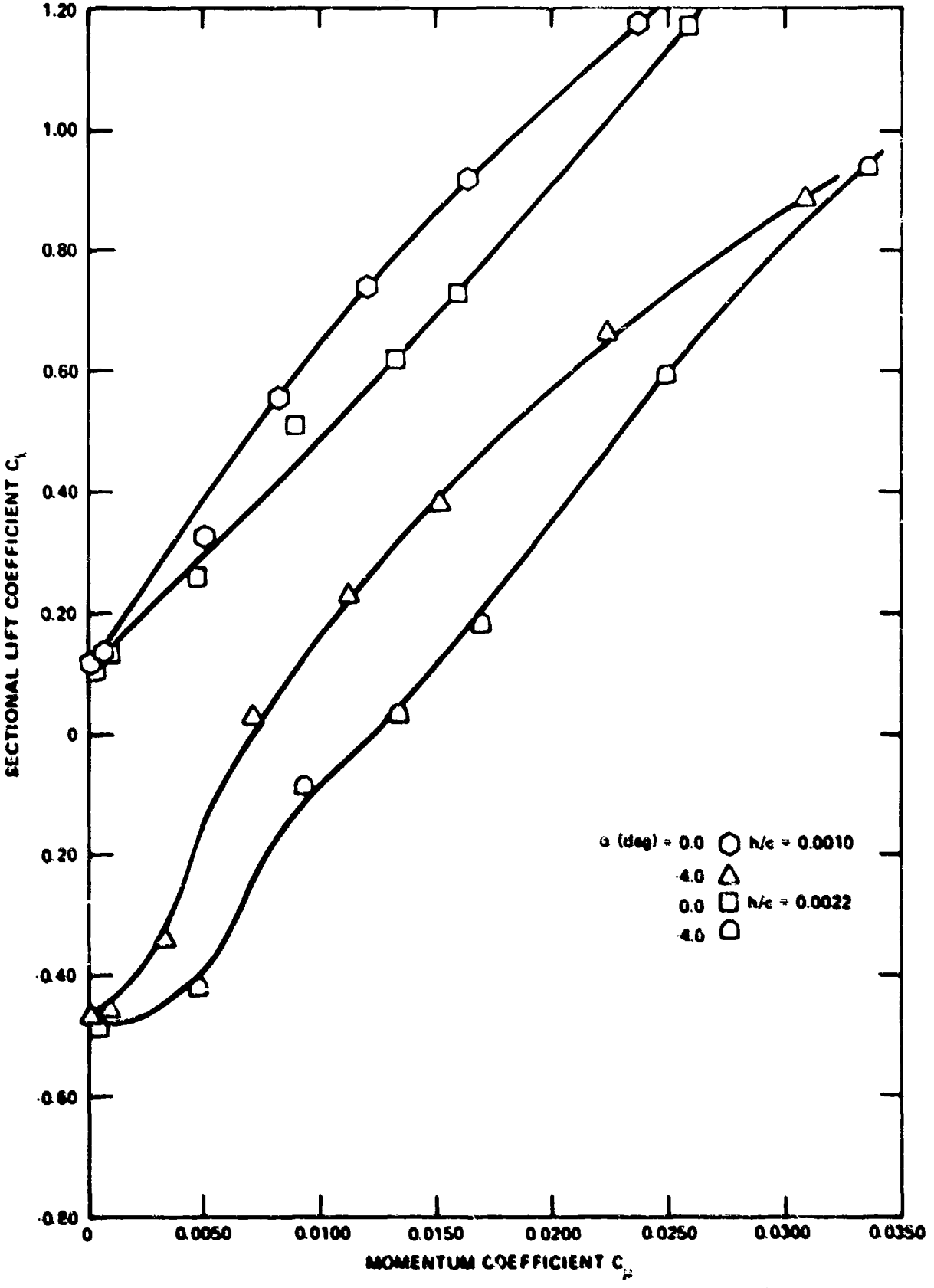

Figure 5d - h/c 0.0010 and 0.0022 (Expanded Scale)

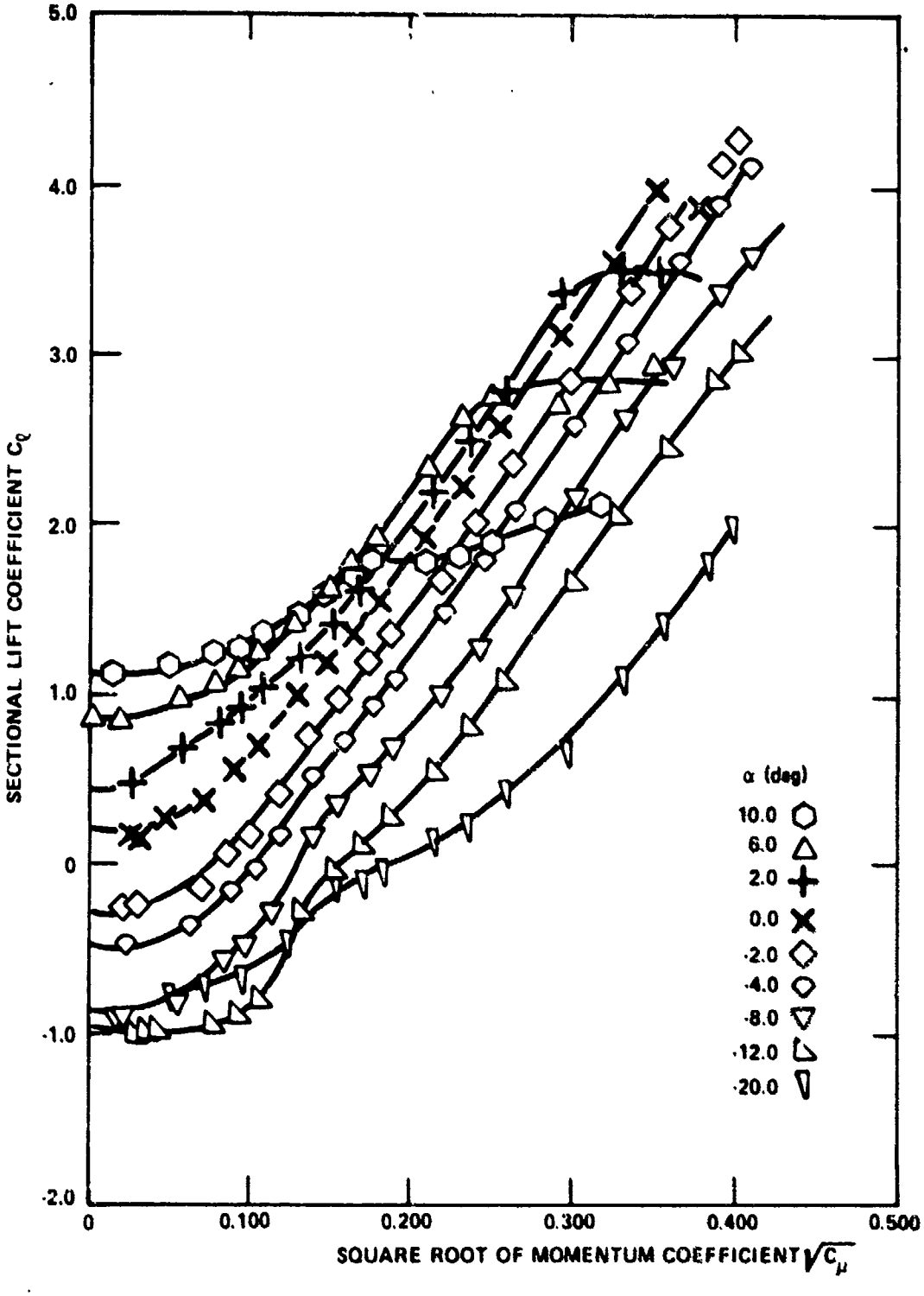

Figure 6 - Lift Variation with the Square Root of Momentum Coefficient

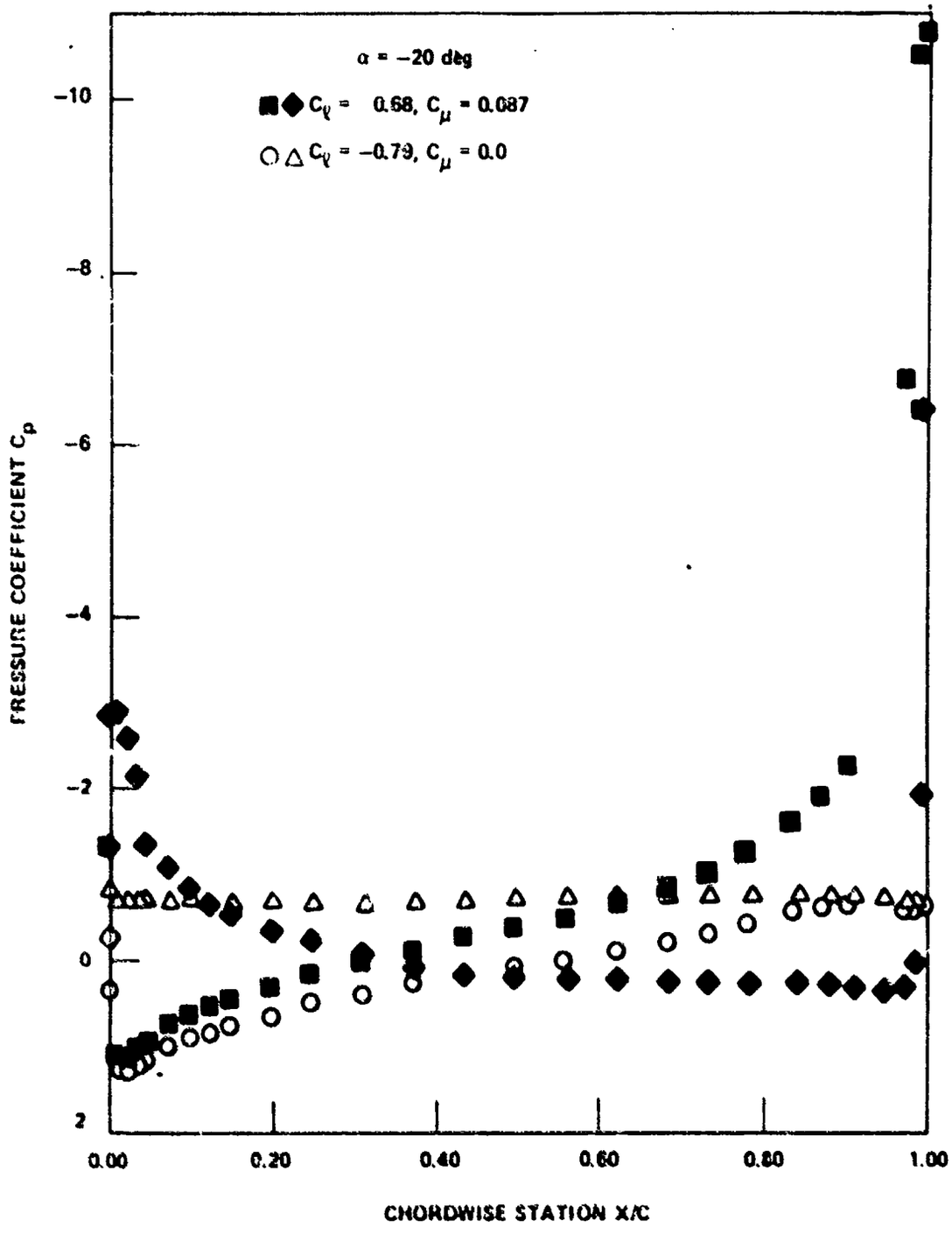

Figure 7 - Experimental Pressure Distributions at α = -20 Degrees

Figure 8 - Variation of Lift Augmentation with Momentum Coefficient

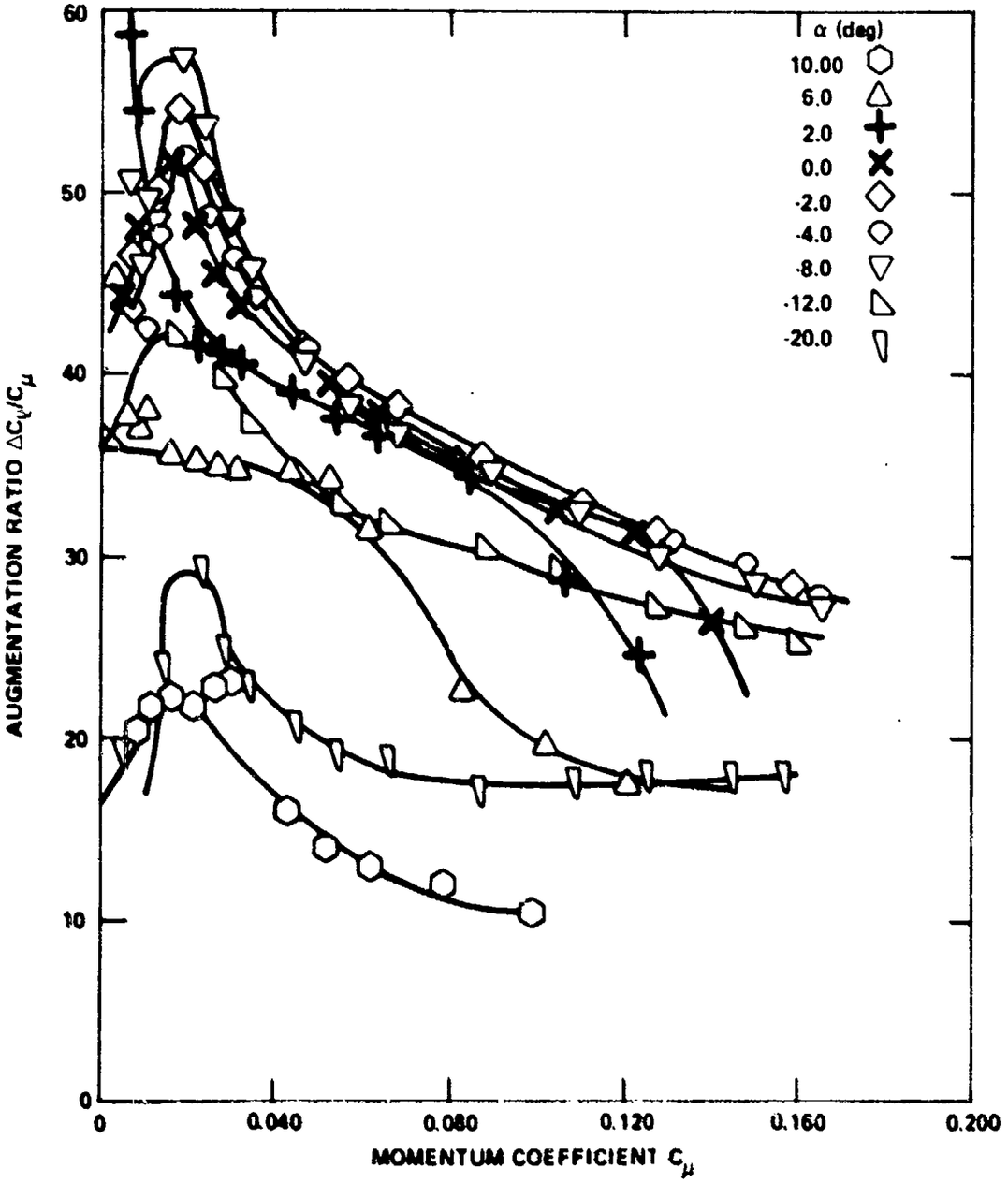

Figure 8a - h/c = 0.0015

Figure 8 (Continued)

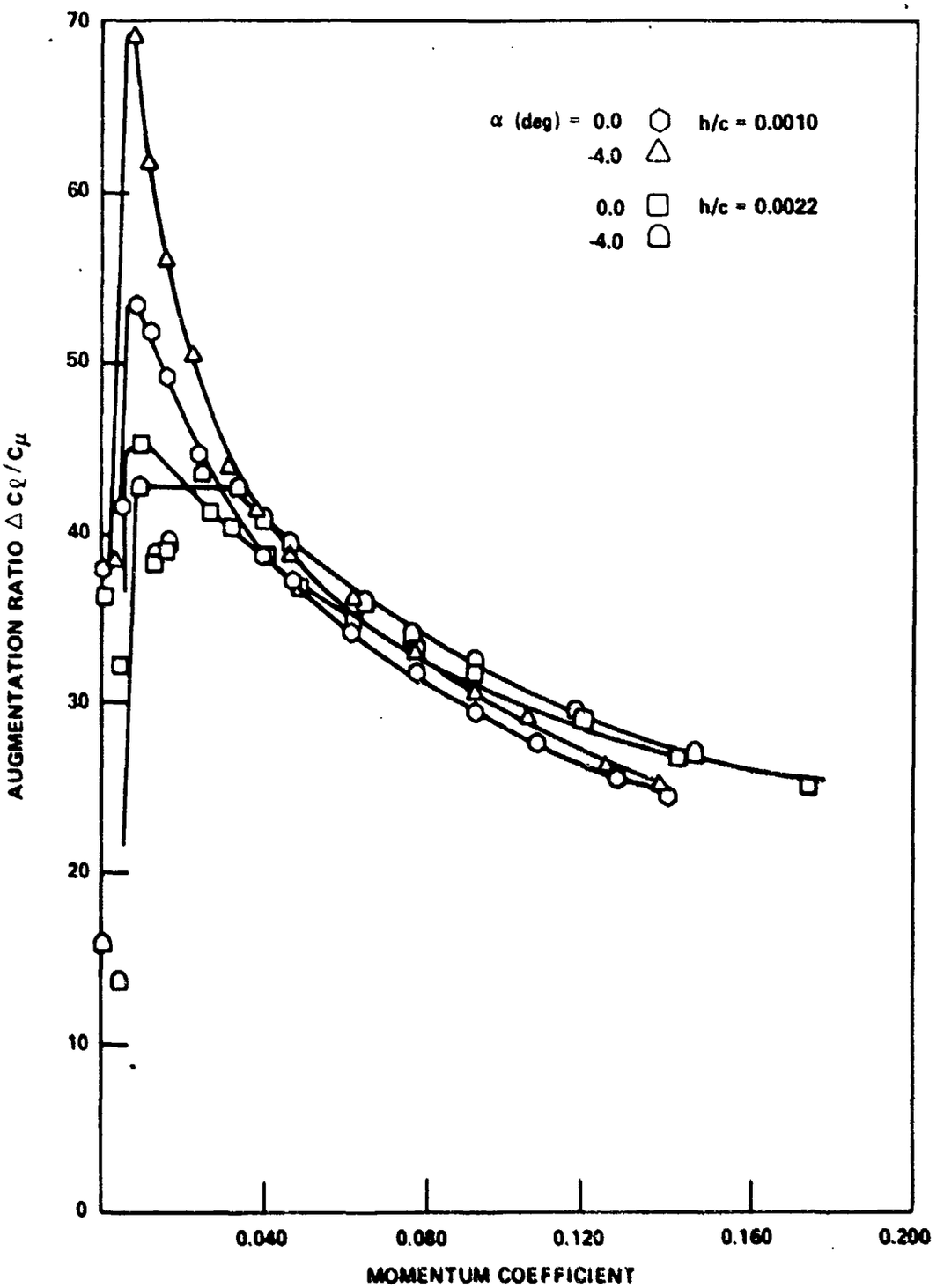

Figure 8b - h/c = 0.0010 and 0.0020

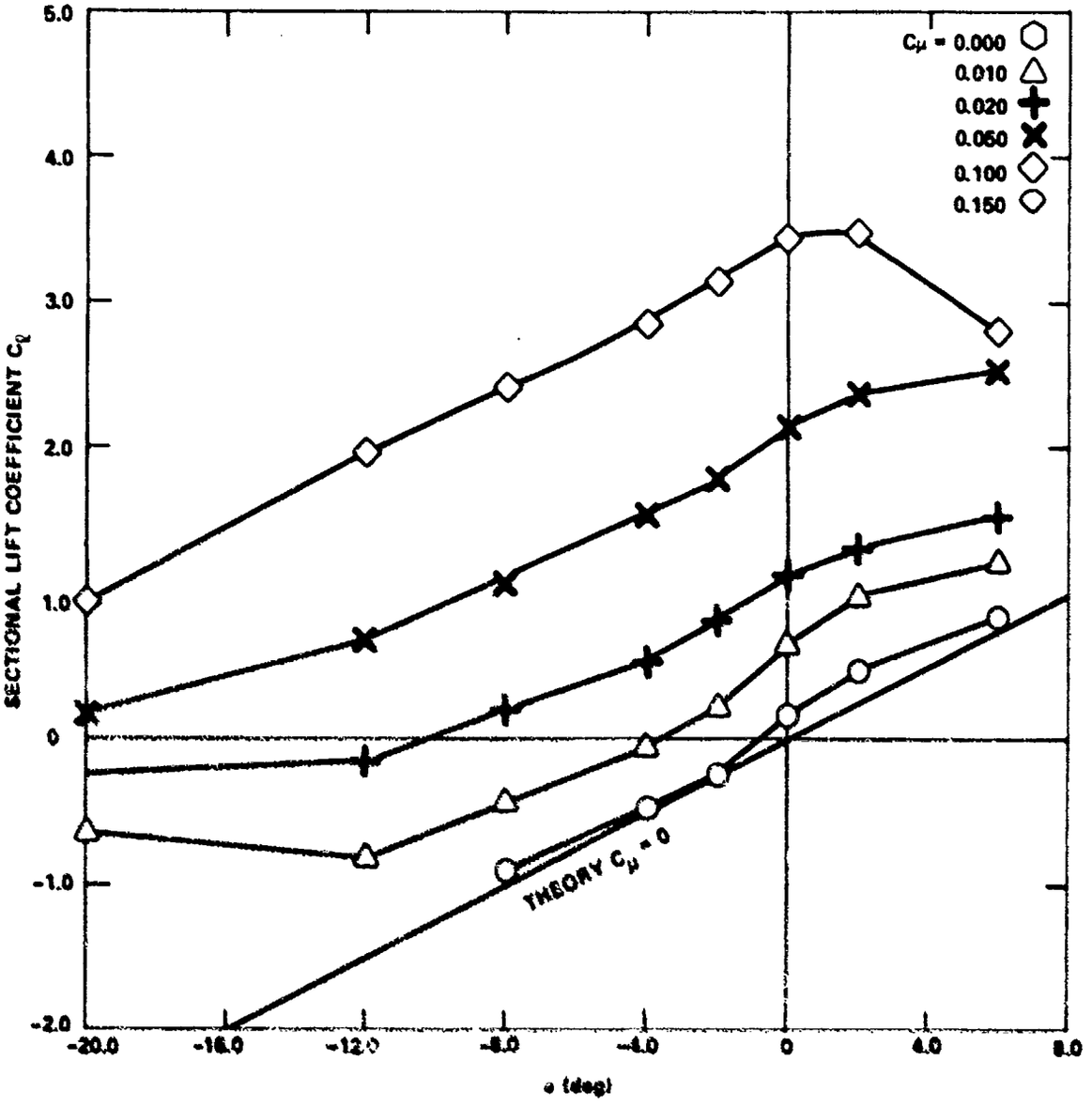

Figure 9 - Lift Variation with Geometric Angle of Attack at h/c = 0.0015

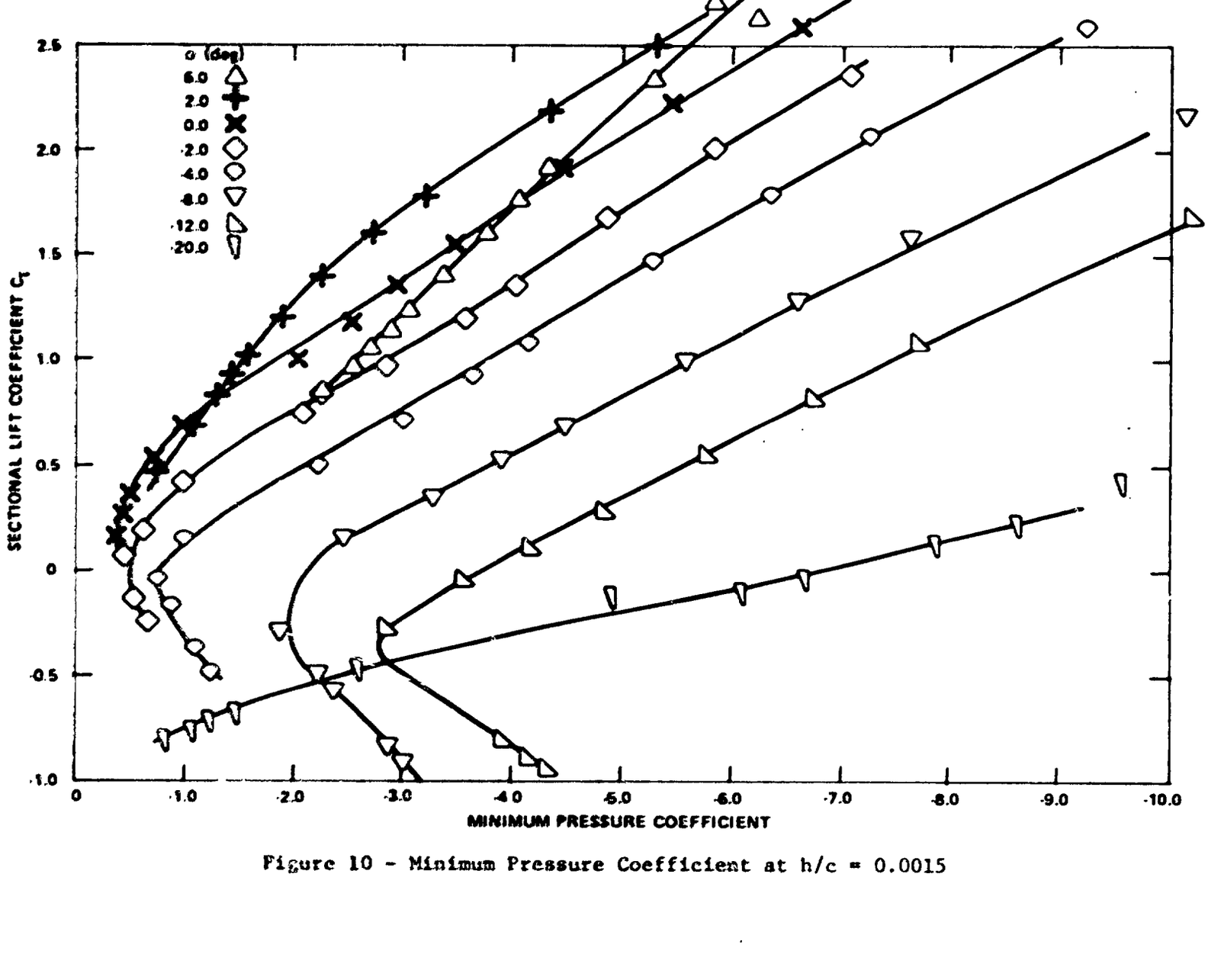

Figure 10 - Minimum Pressure Coefficient at h/c = 0.0015

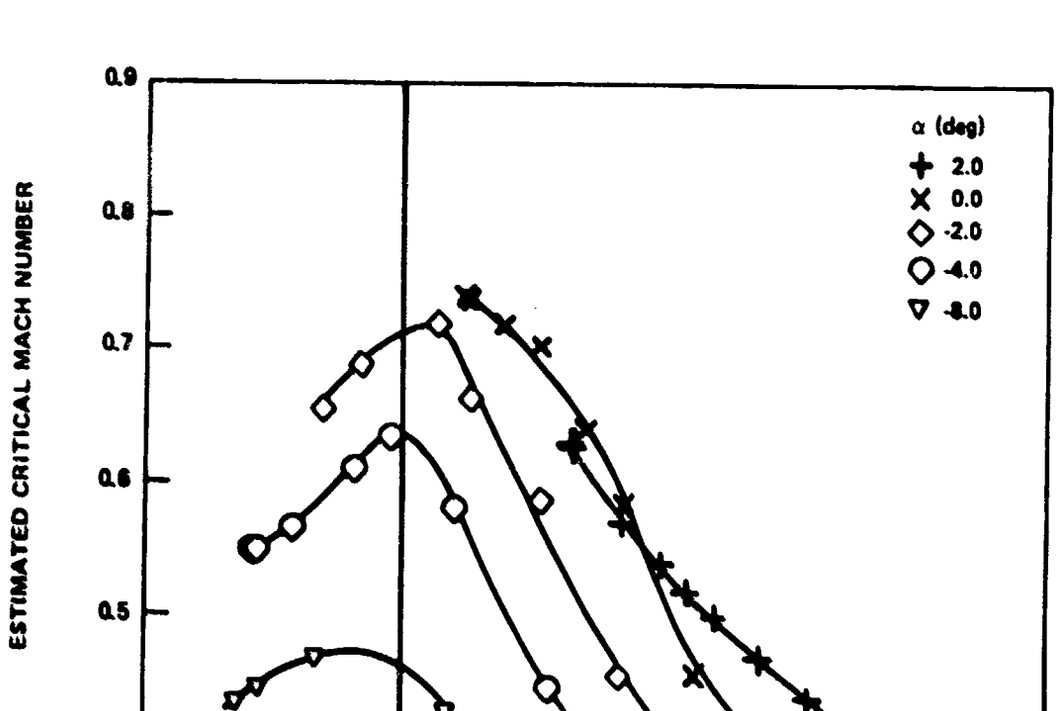

Figure 11 - Variation of Estimated Critical Mach Number with Lift Coefficient

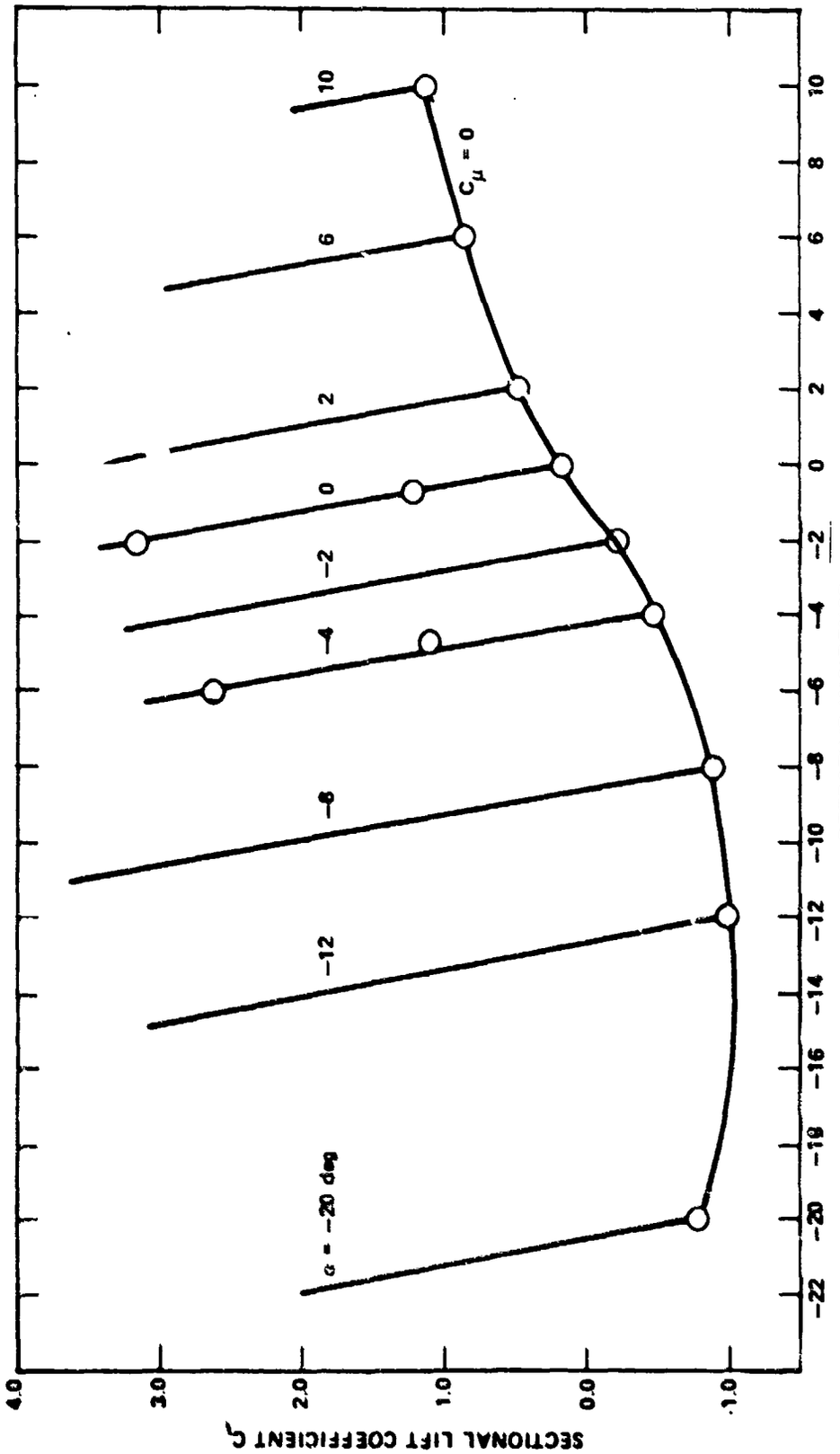

Figure 12 - Induced Angle Correction to Geometric Incidence

Figure 13 - Drag Coefficient Variation with Momentum Coefficient

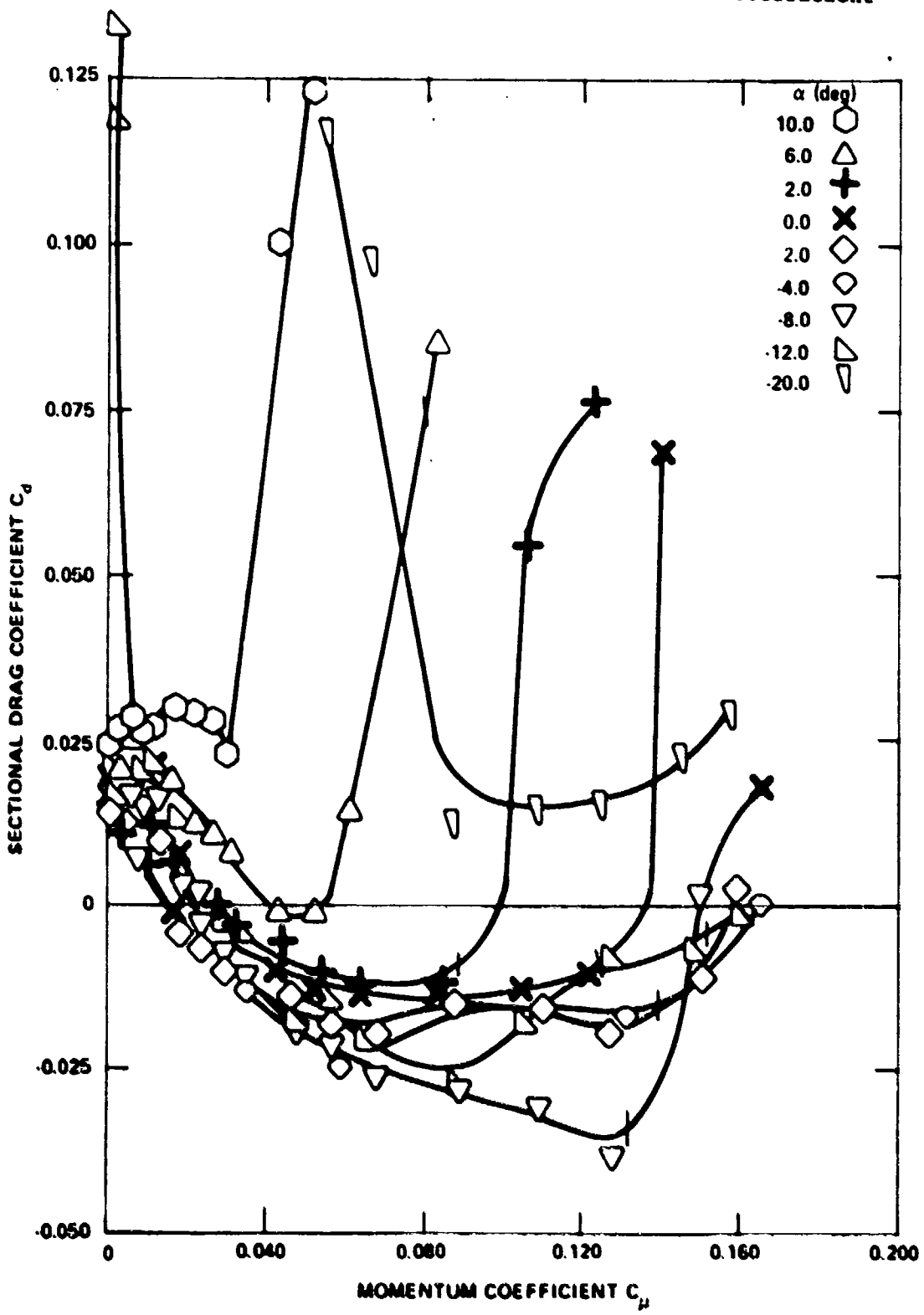

Figure 13a - h/c = 0.0015

Figure 13 (Continued)

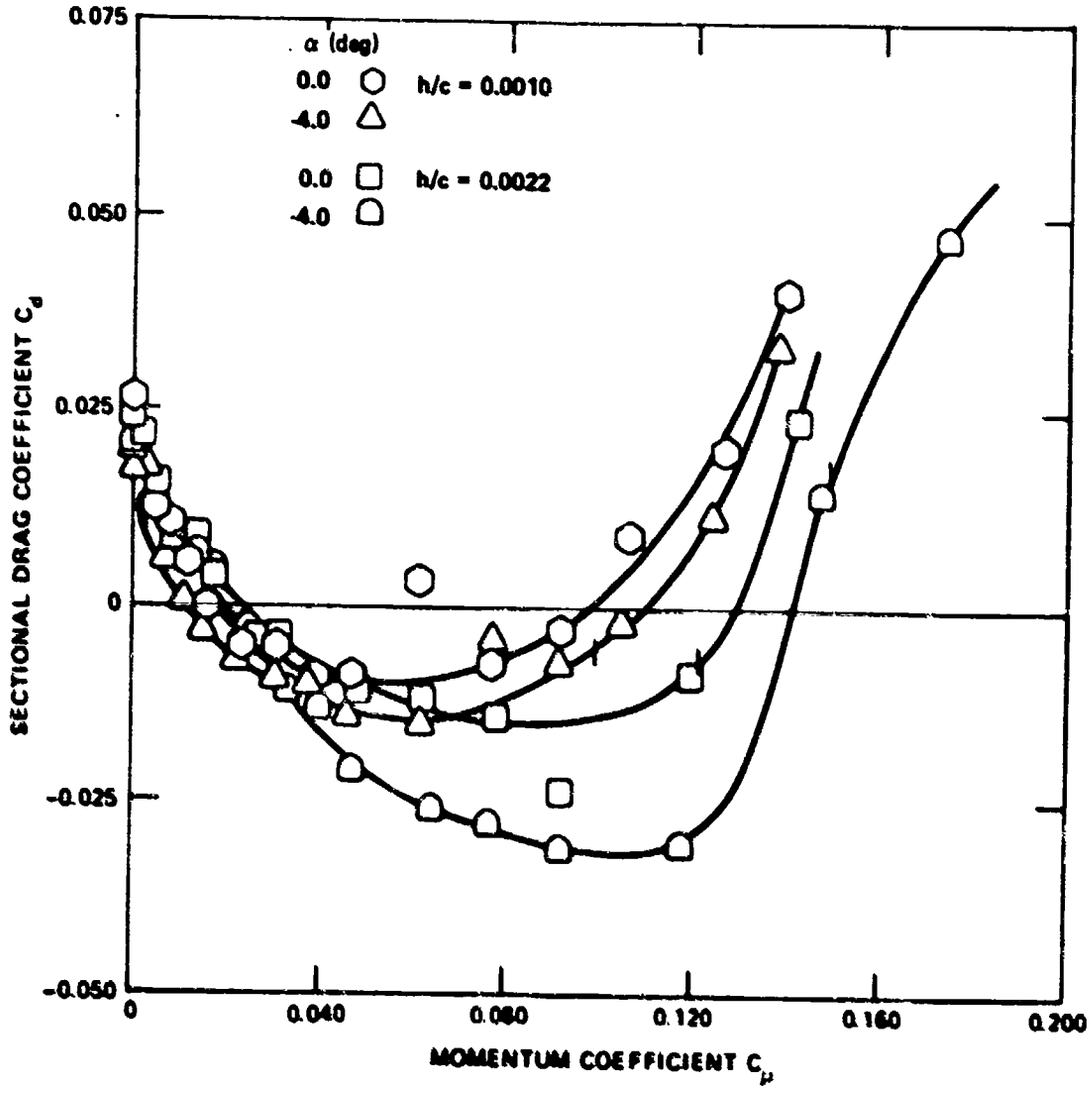

Figure 13b - h/c = 0.0010 and 0.0022

Figure 13 (Continued)

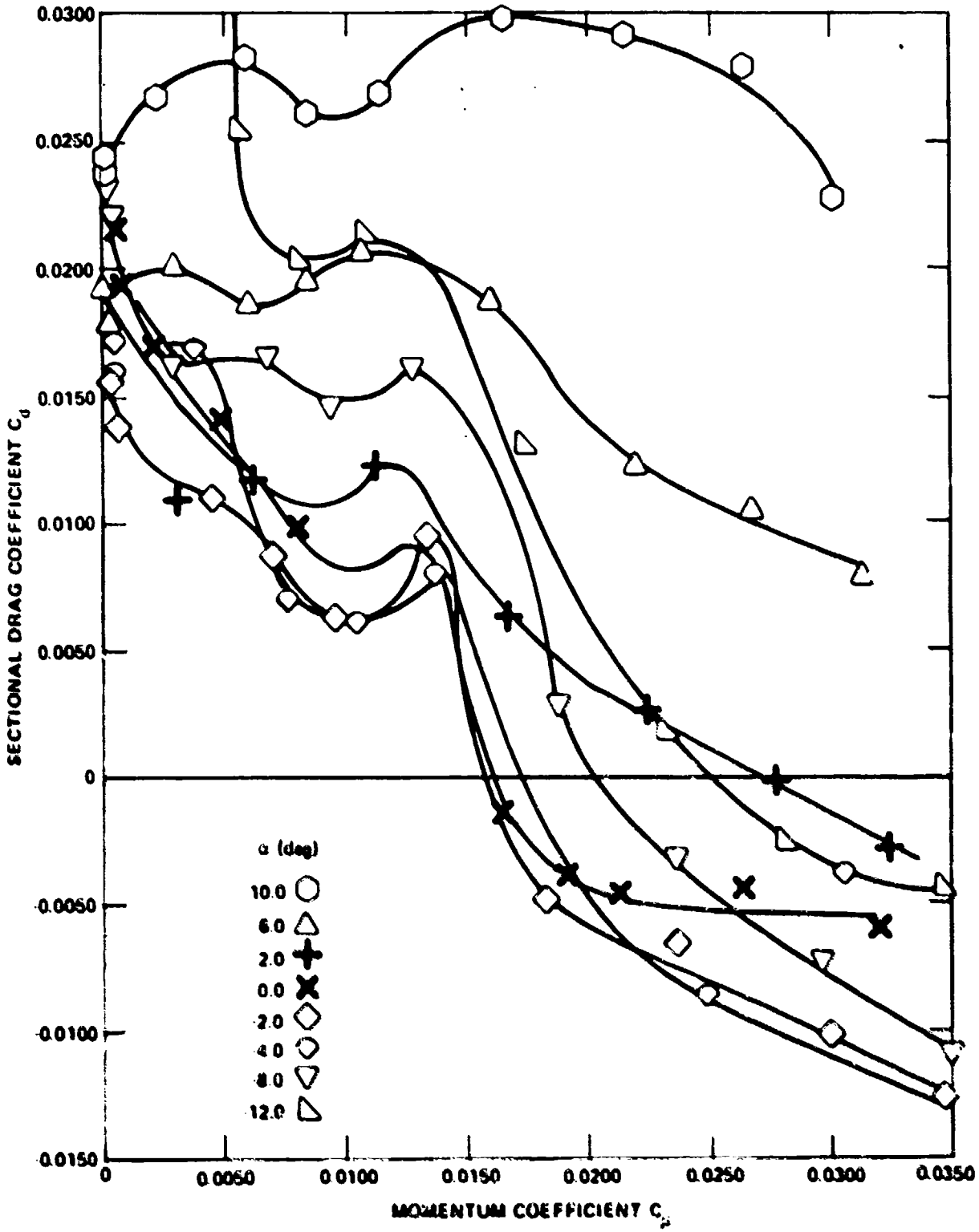

Figure 13c - h/c = 0.0015 (Expanded Scale)

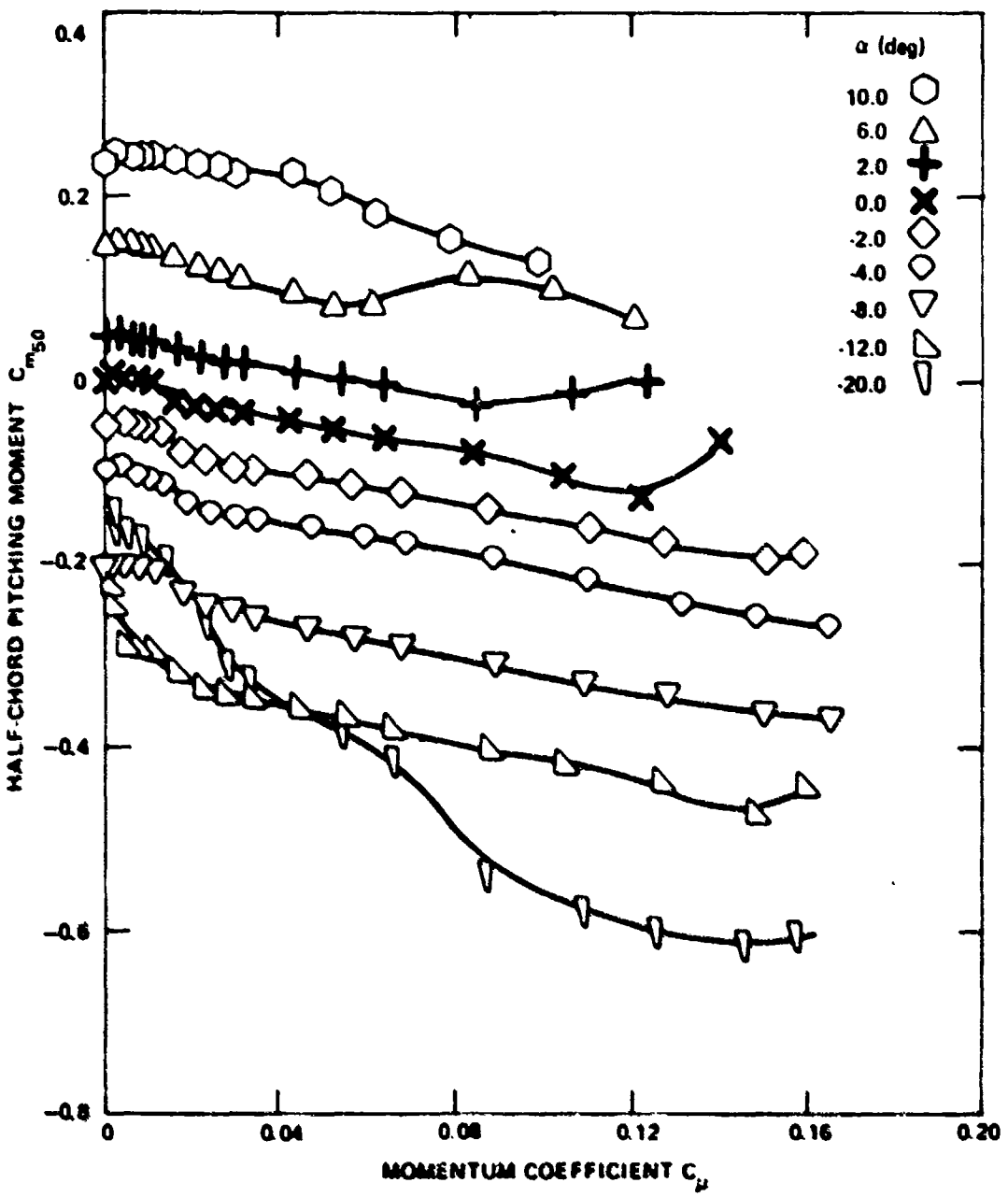

Figure 14 - Variation in Half-Chord Pitching Moment Coefficient at h/c = 0.0015

Figure 15 - Equivalent Lift-to-Drag Ratio

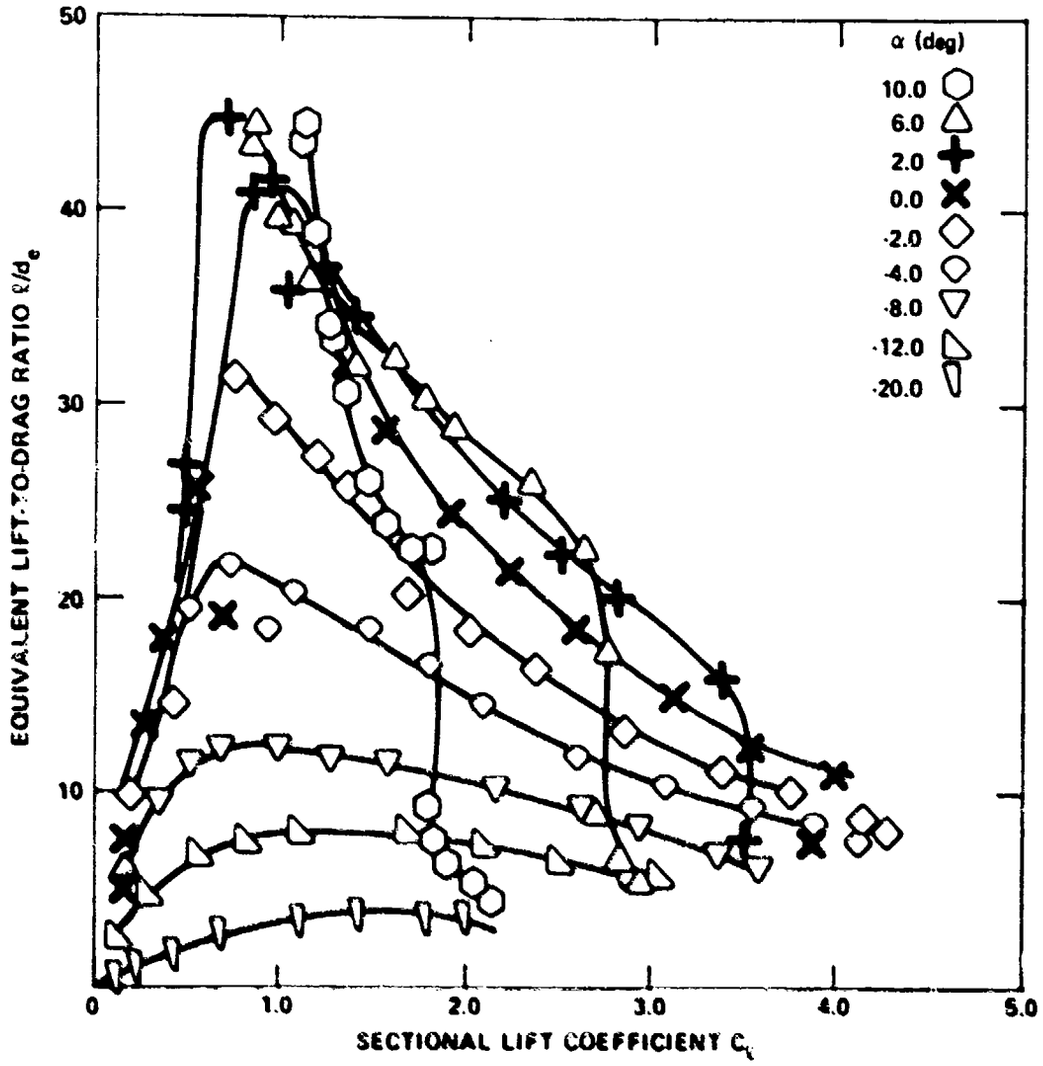

Figure 15a - h/c = 0.0015

Figure 15 (Continued)

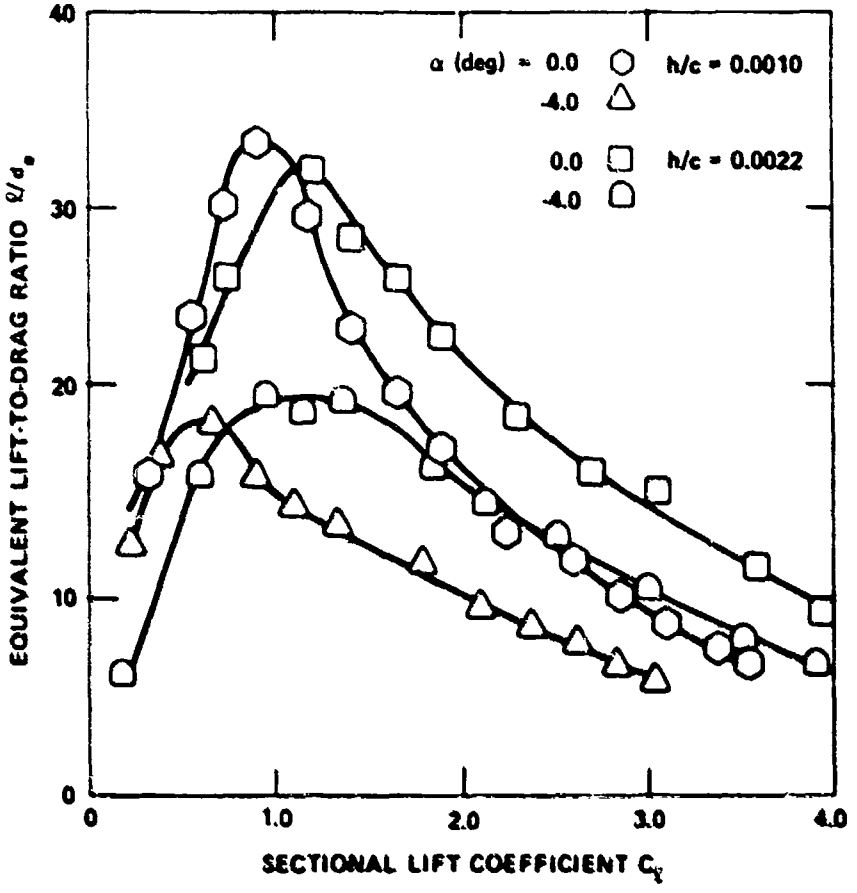

Figure 15b - h/c = 0.0010 and 0.0022

DTNSRDC ISSUES THREE TYPES OF REPORTS

1. DTNSRDC REPORTS, A FORMAL SERIES, CONTAIN INFORMATION OF PERMANENT TECHNICAL VALUE. THEY CARRY A CONSECUTIVE NUMERICAL IDENTIFICATION REGARDLESS OF THEIR CLASSIFICATION OR THE ORIGINATING DEPARTMENT.

2. DEPARTMENTAL REPORTS, A SEMIFORMAL SERIES, CONTAIN INFORMATION OF A PRELIMINARY, TEMPORARY, OR PROPRIETARY NATURE OR OF LIMITED INTEREST OR SIGNIFICANCE. THEY CARRY A DEPARTMENTAL ALPHANUMERICAL IDENTIFICATION.

3. TECHNICAL MEMORANDA, AN INFORMAL SERIES, CONTAIN TECHNICAL DOCUMENTATION OF LIMITED USE AND INTEREST. THEY ARE PRIMARILY WORKING PAPERS INTENDED FOR INTERNAL USE. THEY CARRY AN IDENTIFYING NUMBER WHICH INDICATES THEIR TYPE AND THE NUMERICAL CODE OF THE ORIGINATING DEPARTMENT. ANY DISTRIBUTION OUTSIDE DTNSRDC MUST BE APPROVED BY THE HEAD OF THE ORIGINATING DEPARTMENT ON A CASE-BY-CASE BASIS.